



**CHALMERS**  
UNIVERSITY OF TECHNOLOGY

## **Role of Particle Geometry on the Structural Integrity of Sand and Rock Ilmenite Used as Oxygen Carrier in Combustion of Woody Biomass**

Downloaded from: <https://research.chalmers.se>, 2025-12-09 00:08 UTC

Citation for the original published paper (version of record):

Valizadeh, A., Faust, R., Skoglund, N. et al (2024). Role of Particle Geometry on the Structural Integrity of Sand and Rock Ilmenite Used as Oxygen Carrier in Combustion of Woody Biomass. *Energy & Fuels*, 38(11): 10114-10129.  
<http://dx.doi.org/10.1021/acs.energyfuels.4c00658>

N.B. When citing this work, cite the original published paper.

# Role of Particle Geometry on the Structural Integrity of Sand and Rock Ilmenite Used as Oxygen Carrier in Combustion of Woody Biomass

Ali Valizadeh,\* Robin Faust, Nils Skoglund, Fredrik Forsberg, Marcus Öhman, and Pavleta Knutsson



Cite This: <https://doi.org/10.1021/acs.energyfuels.4c00658>



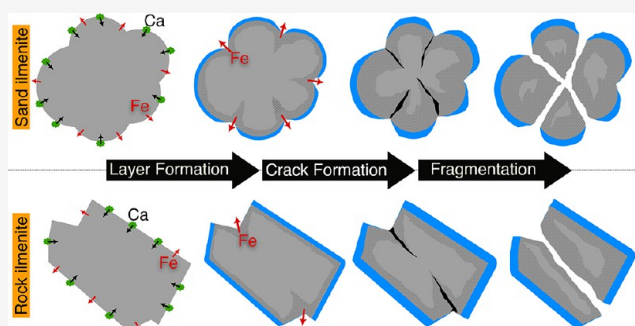
Read Online

ACCESS |

Metrics & More

Article Recommendations

**ABSTRACT:** The role of particle geometry in the structural integrity of sand and rock ilmenite bed particles was studied under prolonged exposure to oxygen carrier-aided combustion (OCAC) conditions in a 12 MW<sub>th</sub> circulating fluidized bed (CFB) boiler. Woody biomass was used as fuel. Bed particles were collected at different stages of the exposure. Fresh bed particles were used as reference samples. All the materials were examined by scanning electron microscopy with energy dispersive X-ray spectroscopy (SEM-EDS) and X-ray microtomography (XMT). The obtained results showed that over time, sphericity diminishes in sand ilmenite, whereas the sphericity of rock ilmenite particles remains unchanged. For both bed types, it was noticed that cracks are mainly connected to the concave areas on the bed particle surface. It was also observed that in sand ilmenite, the bed particle layer predominantly forms on convex areas, resulting in nonuniform distribution, whereas in rock ilmenite, with infrequent convex and concave features, the layer is thicker and exhibits a more uniform distribution. Consequently, the bed particle layer in rock ilmenite plays a higher protection against the outward migration of iron. This, coupled with a lower frequency of concave areas, contributes to a reduced average volume fraction of porous regions and cracks, which makes rock ilmenite structurally more resistant to breakage than sand ilmenite. Notably, the difference in the structural integrity of the two bed types becomes even more pronounced with longer exposure times.



## 1. INTRODUCTION

As global energy demands continue to rise, the criticality of renewable energy sources becomes ever more pronounced.<sup>1–3</sup> Renewable sources not only offer a solution to the declining fossil fuel reserves but also provide an opportunity to reduce carbon emissions, which is a major contributor to climate change.<sup>4–6</sup> In the Nordic countries, the vast forest resources place woody biomass as an important candidate for renewable energy sources.<sup>7–9</sup>

Among different energy conversion technologies, utilizing fluidized beds (FBs) is a favorable technology, particularly for heterogeneous fuels (i.e., woody biomass).<sup>10,11</sup> The strengths of FB include fuel flexibility, allowing a broad range of biomass mixture inputs; low emissions, contributing to cleaner energy conversion; and high efficiency.<sup>11,12</sup> Natural sand, primarily composed of quartz, is the prevalent bed material choice in FBs owing to its low cost and widespread availability.<sup>13</sup> Nonetheless, it interacts with the fuel-derived ash compounds and produces bed and crack layers composed of low-temperature melting silicates.<sup>14</sup> Formation of the bed particle and crack layers makes quartz particles susceptible to bed agglomeration and bed fragmentation, which can potentially lead to serious

operational challenges, including bed defluidization and deposit formation, respectively.<sup>14–16</sup> To mitigate these risks, alternative bed materials have been investigated and implemented. For instance, feldspar and olivine, when used as bed materials, exhibit a significantly lower tendency for agglomerate formation. Recent studies revealed that employing an oxygen carrier (OC) as the bed material in a FB combustion process (also known as oxygen carrier-aided combustion or OCAC) could further enhance the environmental benefits.<sup>17,18</sup> In fact, utilizing the oxygen carrier (e.g., a transition metal oxide) in a single FB reactor mimics the conditions of chemical looping combustion (CLC), where the deliberate separation of air and fuel into two distinct reactors is a key feature aimed at reduced emission.<sup>19,20</sup> In the single reactor scenario, the OC actively transports oxygen from

Received: February 10, 2024

Revised: April 30, 2024

Accepted: April 30, 2024

oxygen-rich to oxygen-lean (fuel-rich) areas within the reactor. Nevertheless, the careful selection of the bed material in OCAC stands as a critical factor in securing both process efficiency and economic feasibility.<sup>21</sup> Given that the majority of evaluated OCs tend to be costlier than conventional bed materials, it is also essential that the selected OC possesses proper mechanical and chemical stability, thereby enhancing the overall system durability.<sup>21,22</sup>

Iron titanium oxide ( $\text{FeTiO}_3$ ), known as ilmenite, stands out as a promising choice among the examined oxygen carriers used as bed materials.<sup>22–24</sup> The chemical interaction between ilmenite and wood fuel-derived ash compounds has been investigated in multiple studies and the bed layer formation on ilmenite bed particles has been explained accordingly.<sup>23</sup> When woody biomass is utilized as fuel, the formation of the bed particle layer starts with the migration of iron from the bed core to the bed surface, which forms porous regions close to the ilmenite surface. Simultaneously, calcium from the fuel ash-forming matter undergoes a solid–solid reaction with ilmenite and produces a thin layer of calcium titanate ( $\text{CaTiO}_3$ ). Therefore, at the early stages of the process, an iron-rich outer layer and a calcium-rich inner layer could be observed on the ilmenite bed particles. As iron is depleted from the bulk material, the porosity beneath the Ca-rich layer increases. Simultaneously, the continuous reduction and oxidation cycles of the bed material gradually build up stress, which, in turn, leads to the eventual formation of cracks in the bed particles. Moreover, the continued incorporation of calcium into the ilmenite structure leads to the thickening of the Ca-rich inner layer and prevents further outward migration of iron. Consequently, there is an observable accumulation of iron beneath the Ca-rich inner layer and within the cracks in the bed particle. In older bed materials, these cracks become pathways for further iron migration toward the bed surface. Furthermore, it was observed that K-compounds migrate into the bed particles and accumulate in the porous regions forming the compound  $\text{KTi}_8\text{O}_{16.5}$  within the bed material.<sup>23,24</sup>

The efficiency of fluidized bed combustion (FBC) systems and their economic viability depend significantly on the choice of bed material. Studies on different bed materials have indicated that the interaction of the fuel-derived ash compounds with bed particles is not solely affected by the changes in the chemical composition of the bed material but also by the changes in surface morphologies of the bed particle.<sup>25–27</sup> For instance, a recent study focusing on ilmenite revealed that the Ca-rich layer tends to form more readily on the convex regions of the particle.<sup>23</sup> This phenomenon leaves the concave regions without a Ca-protection layer, leading to the further depletion of iron from the bed particle core through these areas.<sup>23</sup> This discovery points to the significance of surface morphology in the process, encouraging the exploration of the effect of other physical properties of the bed material that could potentially play a vital role in biomass conversion in an FBC. It has been observed that upon extended exposure, the particles can display softer edges, and their shape becomes more rounded.<sup>24</sup> Thus, in addition to the concave and convex surfaces, particle sphericity may emerge as a particularly important geometric parameter in this context. Sphericity is a dimensionless parameter used to describe the geometry of particles, quantifying how closely the shape of a particle approximates that of a perfect sphere. It is calculated by comparing the surface area of the given particle to that of an ideal sphere with the same volume.<sup>28</sup> Particle sphericity is a

crucial parameter in understanding various characteristics of particles, such as their behavior in fluid flows, packing ability in a volume, and surface interactions.<sup>29,30</sup> Particularly, in the case of bed materials employed within a FB reaction environment, initial particle sphericity as well as sphericity developed throughout the process may offer valuable insights into particle activity and the propensity for attrition or fragmentation.

In previous work, structural changes of ilmenite introduced as sand or crushed rock bed particles from a wood-fired 12 MW<sub>th</sub> circulating fluidized bed (CFB) were studied to compare their mechanical stability as a measure of the life expectancy of these bed material types in industrial application.<sup>21</sup> Although both sand and rock ilmenite possessed identical chemical compositions, they both exhibited distinct morphologies. The particles in the sand ilmenite bed were more rounded, in contrast to the rock ilmenite particles, which featured flat surfaces and sharp edges. SEM cross-sectional images of bed particles taken at different time intervals from the start-up revealed that the mechanical strength of both bed materials is reduced during the combustion process due to the formation of cracks. The crucial difference resided in the fact that sand ilmenite particles fragmented into multiple finer particles as the cracks propagated extensively through the bed particle, while rock ilmenite particles were fractured into larger fragments alongside fewer, yet longer cracks extended through the bed material. Furthermore, according to the same study, the formation of the layer on the bed particles can affect their resistance against attrition and structural degradation.<sup>21</sup> Even though the study pointed to the significance of the structural changes that the ilmenite particles undergo and their importance for the mechanical integrity of the particle, the role of the surface morphology as well as the influence of the ash-layer content on particle stability is left unexplored.

This study aims to address this knowledge gap by investigating morphological changes in ilmenite sand and rock bed particles from the FBC conversion of woody biomass. The impact of surface morphology and particle sphericity (together termed particle geometry) on particle integrity was determined using a combination of X-ray and SEM/EDS analysis techniques. The combination of elemental composition analysis acquired through SEM/EDS, coupled with 3D imaging of bed particles and volumetric analysis conducted via XMT, offered crucial insights into how the geometry of bed particles influences their behavior within the FBC of woody biomass. Results from this work can assist in selecting the proper bed particle type and help to assess the lifetime of the bed particles, which can enhance the economic and environmental viability of the OCAC process.

## 2. MATERIALS AND METHODS

**2.1. Bed Materials.** Ilmenite occurs naturally as sand or as a rock. While sand ilmenite is readily available in various size distributions, rock ilmenite requires mining and crushing to attain the desired size. Consequently, in addition to potential variations in chemical composition depending on the source, these two types of ilmenites also exhibit distinct surface morphologies. In this study, both types of natural ilmenite bed particles were employed as oxygen carrier bed materials (OCs). The sand ilmenite originated from Australia and was supplied by Sibelco, while the rock ilmenite was sourced from Norway and was provided by Titania A/S. X-ray diffraction (XRD) analysis of the fresh sand and rock ilmenite bed particles revealed identical crystal phases in both, with  $\text{FeTiO}_3$  being the primary detected phase. In addition to Fe and Ti serving as the primary constituents, the ilmenite bed materials also featured minor amounts of Mg, Si, Mn, and Ca.

More details on the origin and chemical composition of the utilized bed particle types could be found elsewhere.<sup>21</sup>

**2.2. Fluidized Bed Boiler and Operating Conditions.** The 12 MW<sub>th</sub> CFB boiler with a 2.25 m<sup>2</sup> cross-section and a height of 13.6 m was utilized in this work. A detailed description of the boiler is given elsewhere.<sup>18</sup> Separate experimental campaigns were performed with around 3 tons of bed materials for each ilmenite type. During the experiments, the bed temperature was kept steady at around 850 °C with the boiler being fueled by wood chips having an ash content of 0.4–0.6 wt %. Ash analysis of the utilized fuel is presented in Table 1.

**Table 1. Fuel Ash Composition Was Obtained by ICP-OES Analysis<sup>a</sup>**

	wt % at 550 °C
Ca	26.0
K	12.3
Mg	3.69
Si	2.05
P	2.01
Na	0.79
Mn	0.78
Al	0.44
Fe	0.34
Ba	0.23
Ti	0.04

<sup>a</sup>Reproduced with Permission from ref 21 Copyright 2017 Elsevier.

To maintain stable operating conditions, fresh bed materials were regularly added to keep the bed height constant. The campaign durations were 16 and 14 days for sand and rock ilmenite, respectively. In order to investigate the structural degradation of the bed particles over time, analysis was performed on samples of the fresh bed materials, bed particles taken after 3 days, and the oldest particles collected at the end of each campaign. 0.5–2 kg of bed particles were extracted for each sample from the dense bed with a water-cooled suction tube.

**2.3. Analysis Techniques.** **2.3.1. Scanning Electron Microscopy/Energy Dispersive Spectroscopy Analysis.** To reveal cross-sections of the bed particles for SEM/EDS analysis, ilmenite bed samples were embedded separately in epoxy resin blocks and then dry-polished. The cross-sections were subsequently subjected to analysis through a scanning electron microscope (SEM) utilizing a JSM-IT300 (JEOL, Japan), which was equipped with a backscattered electron detector (BSE) and was operated in low-vacuum mode (100 Pa). For elemental analysis of the bed samples, an X-Max 80 energy dispersive X-ray spectroscopy detector (EDS; Oxford Instruments, UK) was employed. To ensure that the selected bed particles are representative of each sample age, only those with the largest cross-sections, the thickest layer, and the most internal structural changes (compared to the fresh state) were selected for analysis. Approximately, 10 representative bed particles from each sample underwent thorough analysis, encompassing a total of 15–20 spot analyses on each distinctive region within the samples, including the bed particle layer, rigid bed core, porous region, and iron-rich islands, all of which will be discussed in detail later in this paper.

**2.3.2. X-ray Microtomography Analysis.** A Zeiss Xradia 620 Versa X-ray microtomography (XMT) analysis instrument (Carl Zeiss X-ray Microscopy, USA) with a maximum spatial resolution of 0.5 μm was utilized in this study to scan sand and rock ilmenite bed particle samples taken at different time intervals. Kapton tubes featuring an internal diameter of 1 mm were utilized as sample holders. The tube was loaded with bed particles to a height of approximately 2 mm for each bed sample (holding up to 100–150 particles) and was scanned at a resolution (voxel size) of 1.06 μm. All bed samples were scanned under identical parameters, ensuring that the X-ray attenuation across the results remains consistent and comparable. The scanning parameters are listed in Table 2.

**Table 2. X-ray Microtomography Scanning Parameters**

voxel size	1.06 μm
field of view (FOV)	1.07 mm
source	
voltage	50 kV
power	4.5 W
filter	LE2
distance from sample	8.51 mm
Detector	
objective	4X
binning	2
exposure	7 s
projections	3201
distance from sample	46 mm

The tomography reconstructions were performed using the Zeiss reconstruction software, employing the Filtered Back Projection algorithm and utilizing default settings for correcting and removing artifacts. For data evaluation, the reconstructed XMT results were imported into Dragonfly Pro software (Version 2022.2, Object Research Systems (ORS), Canada), enabling both 3D visualization and quantitative analysis.

The time-resolved study required the identification of the oldest particles available at each sampling point. This was made by examining 2D cross-sections along three orthogonal planes within the reconstructed volume. Particles exhibiting the highest degradation and cracks were selected as being the oldest or most typical for each sample age. Subsequently, for each bed sample, five representative bed particles were chosen for further analysis.

**2.3.3. Data Analysis.** Each bed particle was segmented and identified as a unique region of interest (ROI) in Dragonfly. Subsequently, by using the “object analysis” toolbox in Dragonfly, the volume and surface area of each ROI (i.e., each bed particle) were calculated. The calculation process is given in more detail elsewhere.<sup>25</sup>

With the volume ( $V_p$ ) and surface area ( $A_p$ ) of the bed particles determined, the sphericity was calculated using the following equation<sup>31</sup> and subsequently averaged for each bed sample.

$$\text{Sphericity}(\Psi) = \frac{\pi^{1/3}(6V_p)^{2/3}}{A_p}$$

The average specific surface area ( $\tilde{A}_s$ ) of each sample was calculated by dividing each particle's surface area by its volume and then averaging these values across all selected bed particles in the sample.

As the bed materials undergo structural changes throughout the combustion process, distinct regions emerge in the bed particles, each exhibiting unique visual characteristics and chemical composition. The standard thresholding procedure was employed for the identification of these regions.<sup>25</sup> This involved visually comparing XMT images with scanning electron microscopy (SEM) images to select appropriate X-ray attenuation ranges for each region. Subsequently, the particles were segmented into these identified regions. The volume fraction of each region relative to the total volume of the bed particles was then measured and averaged across the entire sample. To determine the average thickness of the bed particle layer for each bed sample, a similar segmentation procedure was employed. The bed particle layer identified in each bed particle was then examined using the thickness measurement toolbox in Dragonfly software.<sup>25,27</sup> More details on the segmentation of different regions in XMT images, as well as the methodologies used for calculating layer thickness and volume fractions, could be found elsewhere.<sup>25</sup>

## 3. RESULTS AND DISCUSSION

**3.1. Bed Particle External Morphology.** Figures 1 and 2 depict the changes in the shapes of typical sand and rock ilmenite bed particles throughout the exposure. These changes

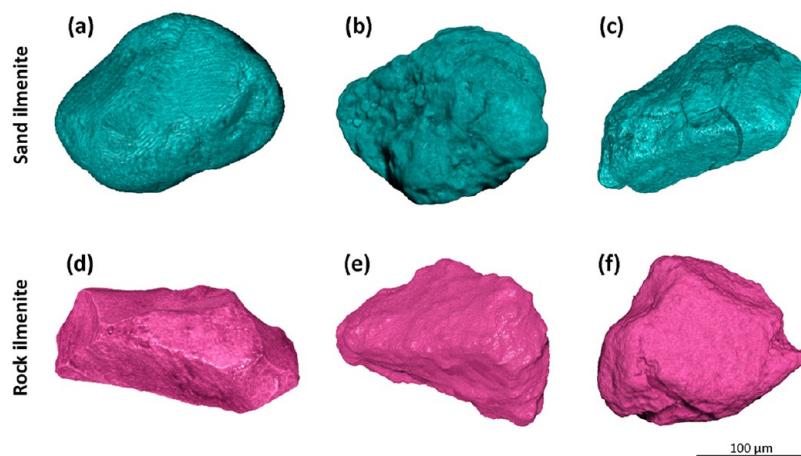


**Figure 1.** 3D XMT images of typical sand ilmenite bed particles taken at (a) the fresh state, (b) 3 days, and (c) 16 days and rock ilmenite bed particles taken at (d) the fresh state, (e) 3 days, and (f) 14 days from the FBC process.

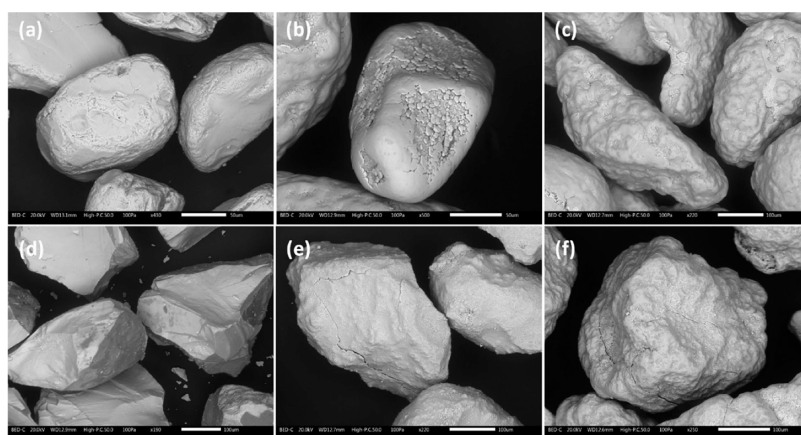


**Figure 2.** Backscattered (BSE) SEM images of the surface of typical sand ilmenite bed particles taken at (a) the fresh state, (b) 3 days, and (c) 14 days and rock ilmenite bed particles taken at (d) the fresh state, (e) 3 days, and (f) 14 days from the FBC process.

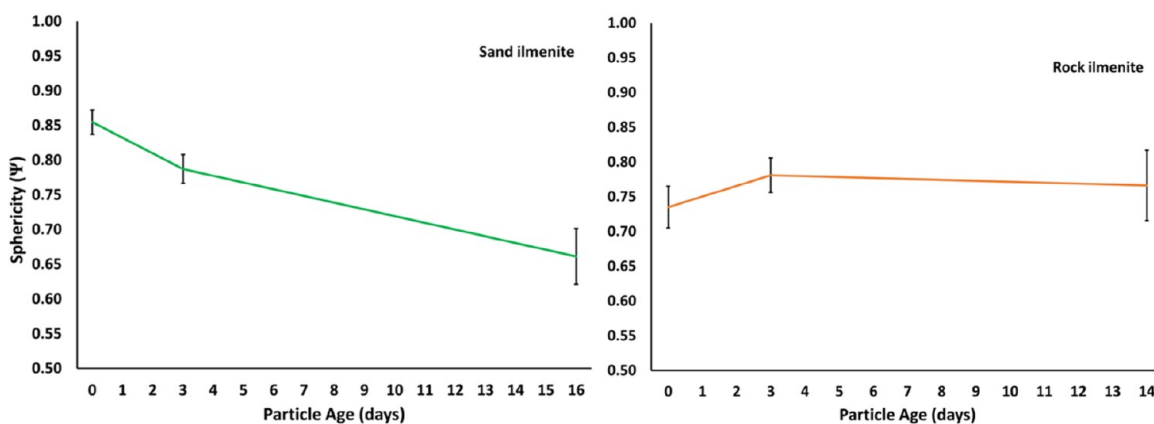


**Figure 3.** Average sphericity of sand ilmenite bed particles taken at the fresh state, after 3 days, and after 16 days and rock ilmenite bed particles taken at the fresh state, after 3 days, and after 14 days from the FBC process measured through XMT analysis. The error bars show 90% confidence interval for the measured data.

are illustrated by using XMT images in Figure 1 and SEM images in Figure 2. Distinct morphological differences could be observed in the fresh state of both bed types. Fresh sand ilmenite particles appear to be more rounded, while rock ilmenite particles exhibit sharp edges and flatter surfaces. As a result of exposure, some of the sand ilmenite particles develop sharp edges and flat surfaces. On the other hand, aged rock

ilmenite bed particles appear to have smoother edges at the end of the exposure. The evolution of distinct physical characteristics of the two types of beds can affect how external forces spread through the particles when they collide with other particles in a fluidized bed environment.<sup>32</sup> Such external forces may lead to the fragmentation of bed particles, particularly in areas that have been weakened (structurally

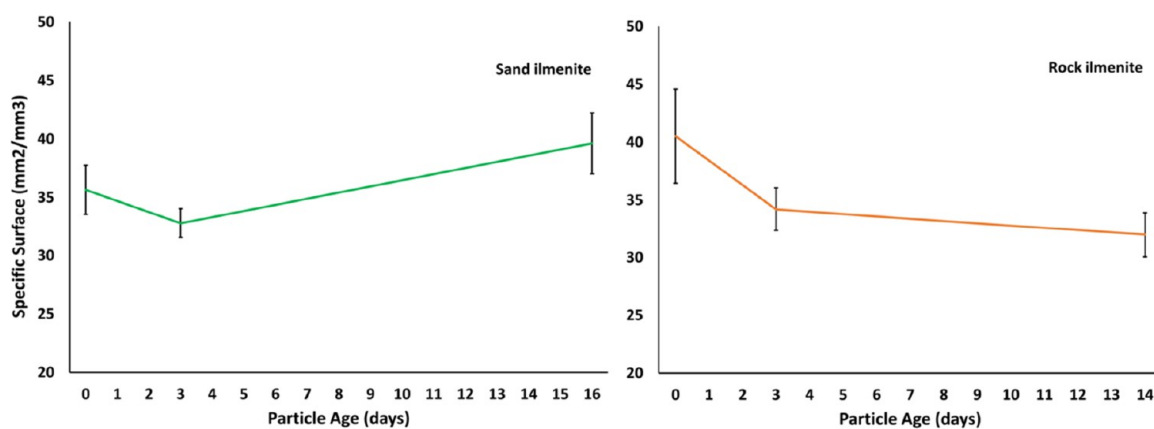


**Figure 4.** Average specific surface area of sand ilmenite bed particles taken at the fresh state, after 3 days and after 16 days, and rock ilmenite bed particles taken at the fresh state, after 3 days and after 14 days from the FBC process measured through XMT analysis. The error bars show 90% confidence interval for the measured data.

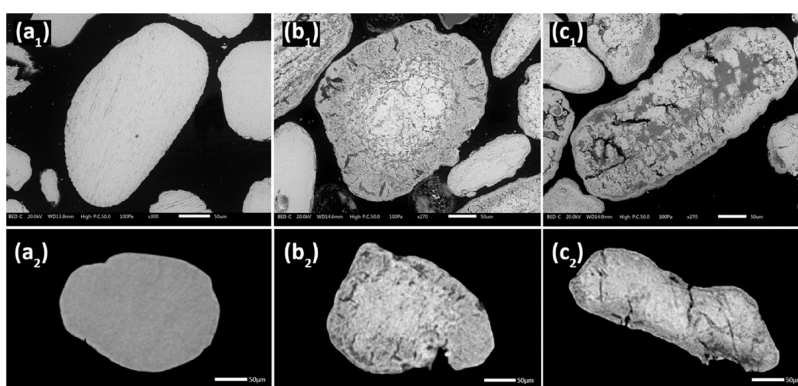


**Figure 5.** Backscattered SEM images (a<sub>1</sub>)–(c<sub>1</sub>) and 2D XMT images (a<sub>2</sub>)–(c<sub>2</sub>) of typical cross-sections of sand ilmenite bed particles taken at the fresh state (a), after 3 days (b), and 16 days (c) from the FBC process.

deteriorated) during the combustion process. Thus, the durability of the bed particles and their resistance to attrition may vary significantly as a result of changes in their surface geometries.<sup>33,34</sup>

Figure 3 represents the development of the average sphericity of the typical bed particles found in sand and rock ilmenite samples. The observed data indicated that fresh sand ilmenite possessed a higher sphericity compared to rock ilmenite, a distinction also visually confirmed in Figures 1 and 2. Performing one-way ANOVA analysis<sup>35</sup> on the time-resolved average sphericity for the two bed types showed that there was no significant difference in the sphericity of rock ilmenite bed particles during the combustion process. In other words, the sphericity of rock ilmenite remained relatively constant over time. Conversely, the analysis revealed that variation in the average sphericity of the sand ilmenite bed particles was statistically significant over time. Postanalysis of the data with the *t*-test method<sup>36</sup> indicated that changes were significant even after 3 days. The decreasing trend in the average sphericity of the sand ilmenite bed particles could be observed in Figure 3. This reduction in sphericity can be attributed primarily to the breakage of the bed particles. As cracks develop internally, they lead to the formation of sharp edges on the fragmented sections, thereby diminishing the overall sphericity of the sand ilmenite particles as they age in the combustion process.

An essential additional aspect to consider following analysis of the sphericity is the specific surface area of the bed particles. This parameter is crucial, as it indicates the extent of surface area for a given volume of bed material with the potential for interaction between the bed material and the fuel-derived ash compounds. The specific surface area is closely interrelated with the sphericity of the particles.<sup>37</sup> Generally, particles with higher sphericity, resembling more spherical shapes, tend to have a lower specific surface area due to the geometrical characteristic of spheres having the least surface area for a given volume. Conversely, particles with lower sphericity, exhibiting more irregular or elongated shapes, are associated with a higher specific surface area. In practical applications, this means that changes in sphericity due to processes such as attrition, fragmentation, or agglomeration can directly impact the specific surface area and, consequently, the behavior and effectiveness of the bed particles.

Figure 4 illustrates variations of the average specific surface area for both rock and sand ilmenite bed particles. From the figure, it can be seen that the trend is mirroring that observed for the sphericity. The results of the one-way ANOVA analysis indicate that variation in the average specific surface area for rock ilmenite bed particles was not significant over time. In contrast, the analysis demonstrates statistically significant changes in the average specific surface area for the sand ilmenite bed particles. Subsequent analysis using the *t*-test method revealed that the variation was not significant between

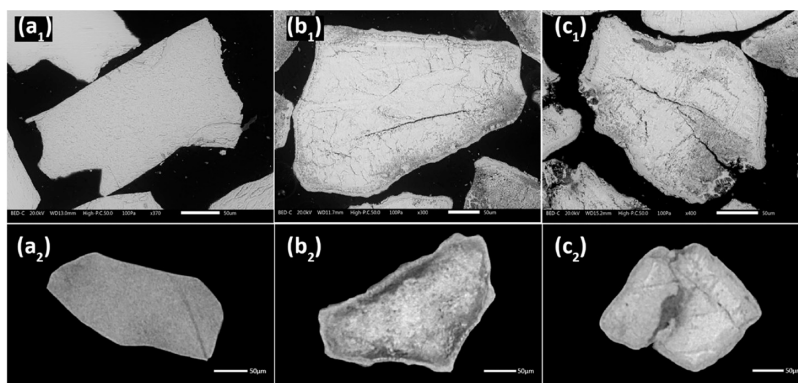


**Figure 6.** Backscattered SEM images (a<sub>1</sub>)–(c<sub>1</sub>) and 2D X-ray microtomography images (a<sub>2</sub>)–(c<sub>2</sub>) of typical cross-sections of rock ilmenite bed particles taken at the fresh state (a), after 3 days (b), and 14 days (c) from the FBC process.

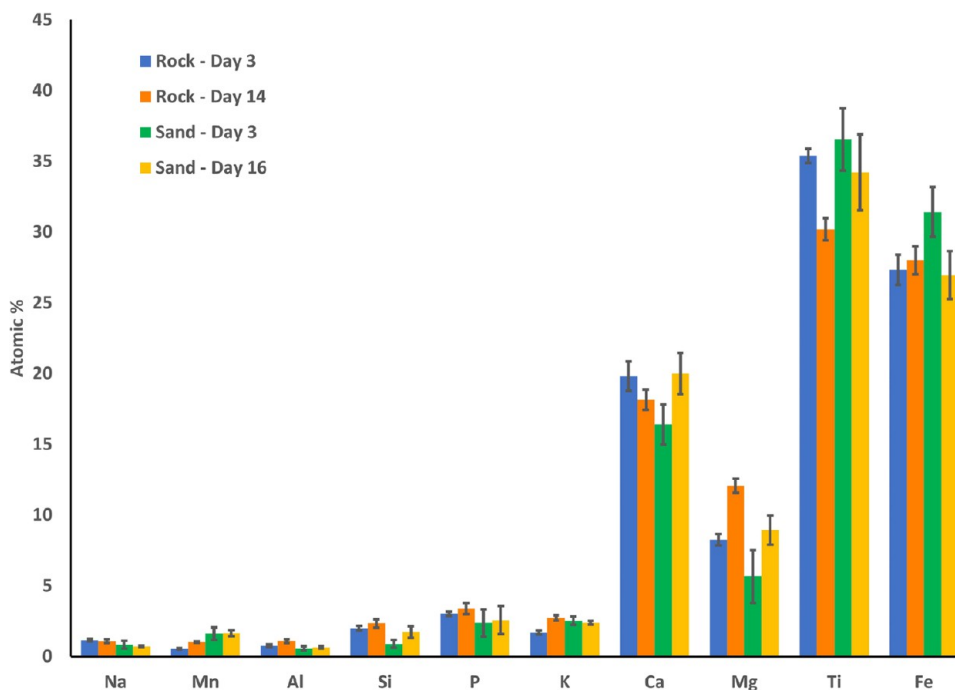


**Figure 7.** Average elemental composition of bed particle layer on sand ilmenite bed samples taken after 3 and 16 days and rock ilmenite bed samples taken after 3 and 14 days from the FBC process. The values are on a C- and O-free basis, presented in at%, and obtained through SEM-EDS. The error bars show 90% confidence interval for the measured data.

the fresh particles and those taken after 3 days but was significant for the older particles. This uptrend for sand ilmenite bed particles can be observed in Figure 4 and indicates an enhanced potential for interactions with the fuel-derived ash compounds in aged sand ilmenite particles, which might further result in faster degradation of these bed particles over extended time periods in the combustion process compared to the rock ilmenite particles.

**3.2. Bed Particle Internal Morphology.** SEM and XMT images in Figures 5 and 6 exhibit cross-sections of typical sand and rock ilmenite bed particles taken at selected time intervals from the combustion process. These images provide a visual representation of the structural changes in the bed particles over time. Both bed materials possessed an almost homogeneous internal structure in their fresh state (Figures 5a and 6a). Changes in the bed particle structure could be observed on day 3. These structural changes could be categorized into bed particle layer formation and internal alterations and will be

discussed in detail in the following subsections. Upon comparison of images obtained through SEM and XMT, a visible resemblance in the visual representation of various regions within the bed particles could be observed across both characterization techniques.

**3.2.1. Bed Particle Layer Formation.** After 3 days of exposure, formation of the bed particle layer on both sand and ilmenite particles could be observed (Figures 5b, 6b, 8c, and 9c). The average elemental compositions of the bed particle layer for both bed types over time are presented in Figure 7. EDS analysis of the surface layer on both bed types indicated a predominance of calcium (Ca) and titanium (Ti) in nearly equimolar ratios. This composition aligns with the formation of  $\text{CaTiO}_3$ , a phase frequently identified in X-ray diffraction (XRD) analyses of used ilmenite.<sup>23,24</sup>  $\text{CaTiO}_3$  is known for its tendency to form solid solutions with magnesium, which explains the elevated levels of Mg detected in the particle layer. In addition to Mg, Ca, and Ti, iron (Fe) was also a significant

component of the formed layer. Fe is commonly observed to migrate toward the surface of the bed particles, forming hematite or magnetite, which plays a crucial role in the oxygen-carrying capacity of the bed material.<sup>23,24</sup>

Despite the similarity in chemical composition, the layer on sand ilmenite was thicker in the convex parts of the bed particles and was thinner or absent in the concave areas (Figure 8). In contrast, the bed particle layer on rock ilmenite

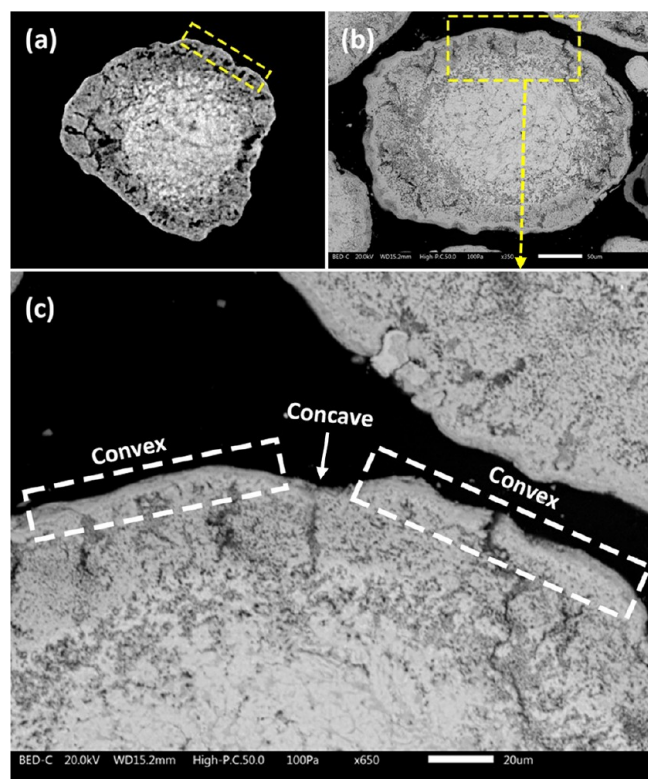


**Figure 8.** 2D XMT image (a) and 2D backscattered SEM images (b and c), of typical cross-sections of sand ilmenite taken after 3 days from the fluidized bed combustion process. The yellow dashed area in (b) is magnified in (c).

particles appeared to be more uniform and covered almost the entire surface of the particles (Figure 9). The observed variation in layer formation on convex and concave surfaces of the bed particles aligns with findings reported in previous research.<sup>23,25–27</sup>

Figure 10 shows the evolution of the average layer thickness measured for both rock and sand ilmenite bed particles throughout the combustion process. After 3 days, rock ilmenite showed a marginally higher particle layer thickness compared to that of sand ilmenite. Cross-sectional SEM images of the bed particles (Figures 8 and 9) also showed that the bed particle on rock ilmenite was distributed more uniformly on the particle surface compared to that of sand ilmenite.

Performing a *t*-test indicated that there was no significant difference in the average bed particle layer thickness for sand ilmenite after 3 days. However, a significant difference was observed in the average values for rock ilmenite measured after 3 and 14 days. For the longest exposed particles (after 14 days), the average layer thickness in rock ilmenite was lower than that measured for younger bed particles (after 3 days), which agrees with the previous findings that rock ilmenite

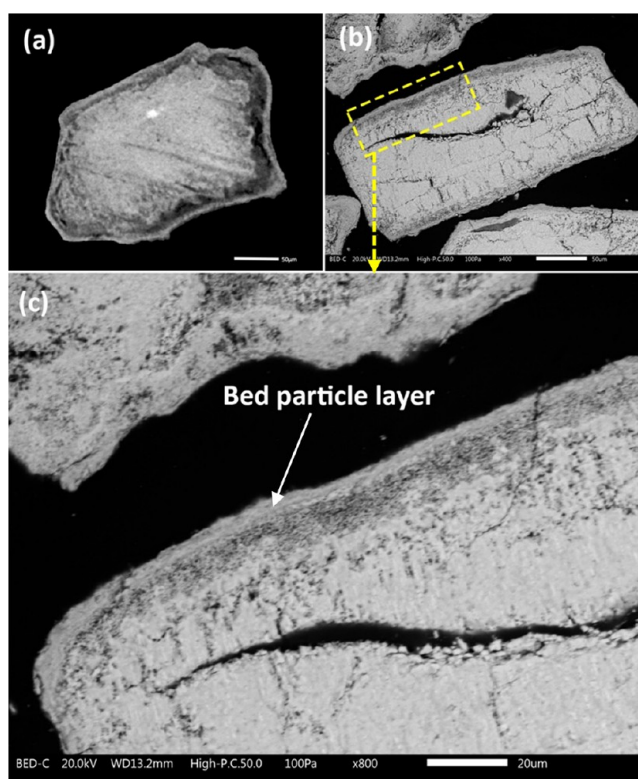


**Figure 9.** 2D XMT image (a) and 2D backscattered SEM images (b and c), of typical cross-sections of rock ilmenite taken after 3 days from the fluidized bed combustion process. The yellow dashed area in (b) is shown magnified in (c).

experiences higher surface attrition compared to sand ilmenite.<sup>21</sup>

**3.2.2. Internal Structural Changes.** Within the core of the bed particle, three distinct areas defined by different shades of gray are observable, namely, rigid bed core, porous regions, and iron-rich islands). These regions (highlighted for both bed types in Figure 11) are identified based on data on ilmenite bed particles from previous studies,<sup>21,23</sup> combined with current data collected from backscattered SEM images and EDS data. The presence of the three regions was consistent across different types and ages of the analyzed bed materials, although the extents of each of the phases varied among the samples. In addition to the development of the three distinct regions mentioned above, formation and propagation of cracks were also observed in both bed types.

By comparison of 2D XMT images with cross-sectional SEM images of the bed particles, along with the insights provided by EDS analysis, corresponding X-ray attenuation ranges were selected to identify the aforementioned regions together with the bed particle layer and the cracks in the XMT images. The different segments defined in the bed particles are demonstrated in 2D in Figure 12.

**3.2.2.1. Porous Regions.** After 3 days, the porous regions, which appeared darker in the images, were predominantly situated beneath the formed layer (Figures 5b and 6b). In the longest exposed particles, as can be perceived from Figures 5c and 6c, these regions had expanded more extensively throughout the bed material. Formation of the porous regions in ilmenite bed particles has been repeatedly reported by researchers.<sup>21,23,24</sup> This phenomenon is attributed to the preferential migration of iron (Fe) from the particle core

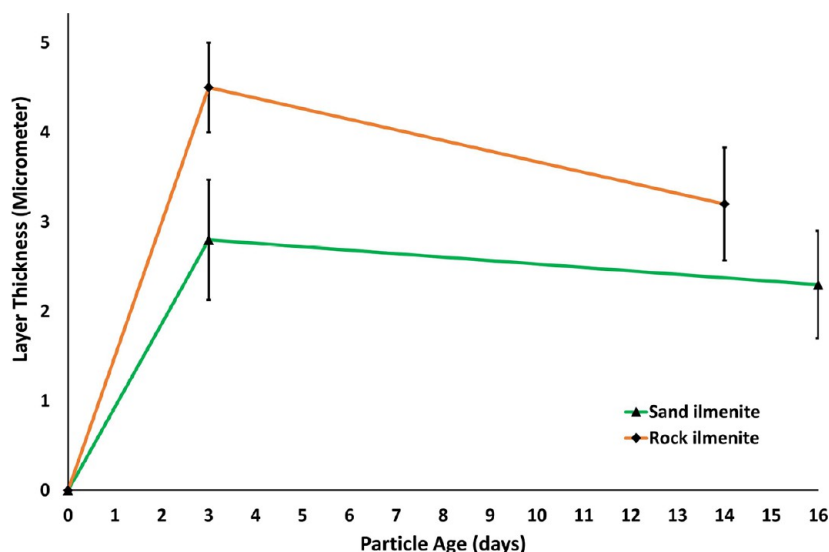


**Figure 10.** Average bed particle layer thickness of sand ilmenite bed particles taken at the fresh state, after 3 days and after 16 days, and rock ilmenite bed particles taken at the fresh state, after 3 days and after 14 days from the fluidized bed combustion process measured with XMT analysis. The error bars show 90% confidence interval for the measured data.

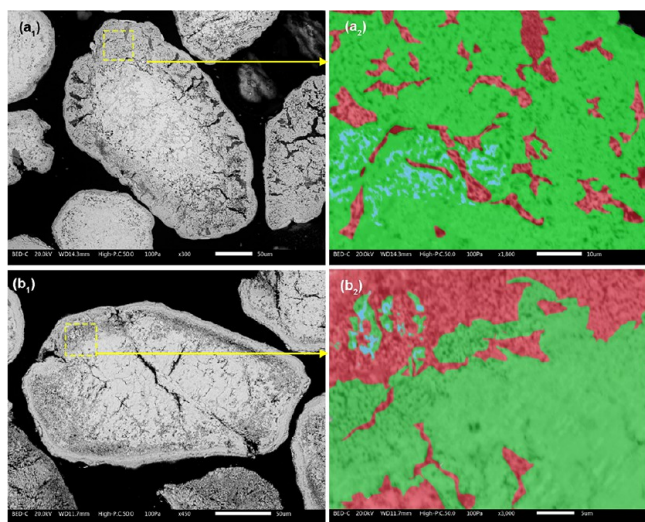


**Figure 11.** 2D backscattered SEM images of typical cross-sections of sand ilmenite ( $a_1$ ), and rock ilmenite ( $b_1$ ) taken after 3 days from the fluidized bed combustion process. The colors highlighted in figures  $a_2$  and  $b_2$  show three distinct regions identified in the bed core: green (rigid bed core), red (porous regions), and blue (iron-rich islands).

toward the surface and a higher partial pressure of oxygen. As iron atoms migrate, they create vacancies behind them that can accumulate and form porous regions. Therefore, as it could also be perceived from Figure 13, the concentration of iron in these regions was noticeably lower than that in fresh ilmenite. Porous regions are further characterized by their high concentrations of K and Ti. This specific elemental composition is indicative of the K-titanate phase, which is commonly observed in ilmenite that has undergone interaction with the wood-derived ash compounds.<sup>24</sup> The observations also confirm the higher tendency of potassium to penetrate into the bed particle core as opposed to calcium.

Figure 14 provides a visual representation of how porosity evolved over time within both sand and rock ilmenite bed particles. It is evident from the figure that sand ilmenite exhibited a higher volume fraction of the porous region compared to that of rock ilmenite. However, ANOVA analysis showed that for both bed types, there was a significant difference in the average volume fraction of the porous region over time. Further, performing a *t*-test indicated that there was no significant difference in the values after 3 days. This means that for both bed types, the majority of the porosity

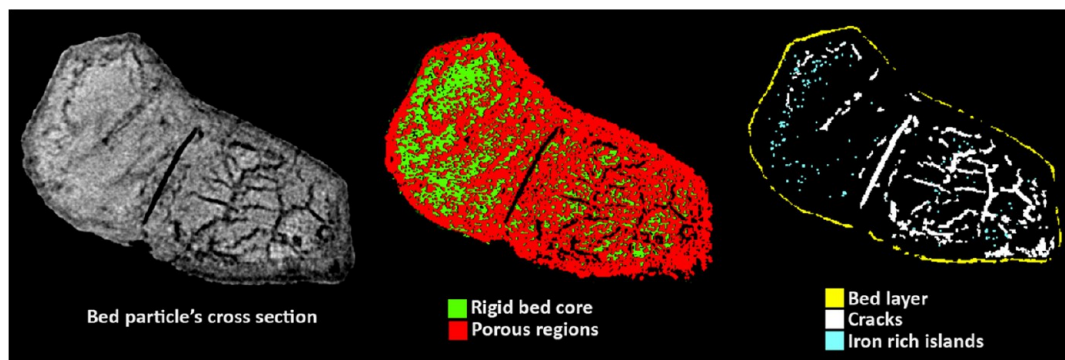


**Figure 12.** Segmentation of porous regions (red), rigid bed core (green), bed particle layer (yellow), cracks (white), and iron-rich islands (blue) found in a cross-sectional XMT image of a typical sand ilmenite bed particle taken after 16 days from the FBC process.

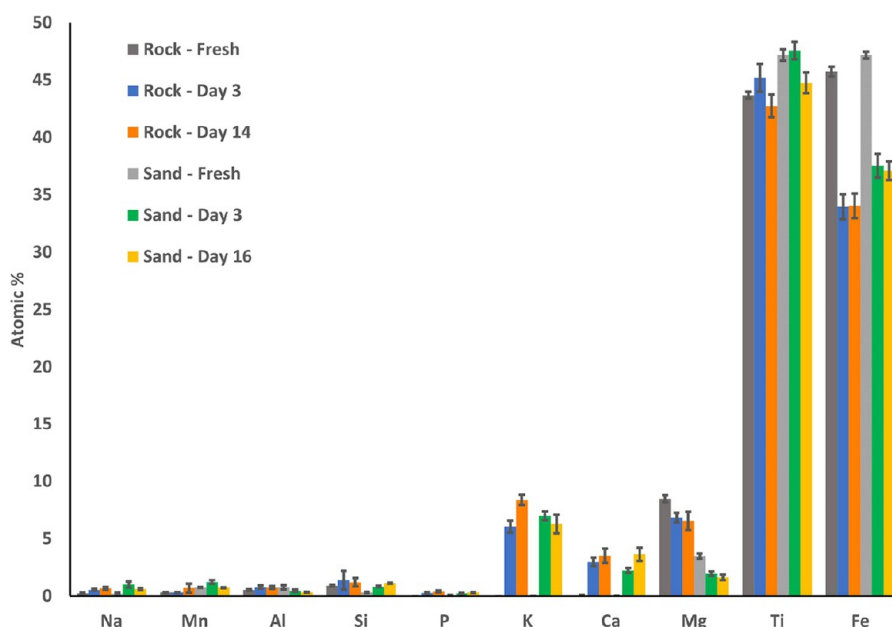


**Figure 13.** Average elemental composition of the fresh bed materials, porous regions in sand ilmenite bed samples taken after 3 and 16 days, and porous regions in rock ilmenite bed samples taken after 3 and 14 days from the FBC process. The values are on a C- and O-free basis, presented in at%, and obtained through SEM-EDS. Error bars show 90% confidence interval for the measured data.

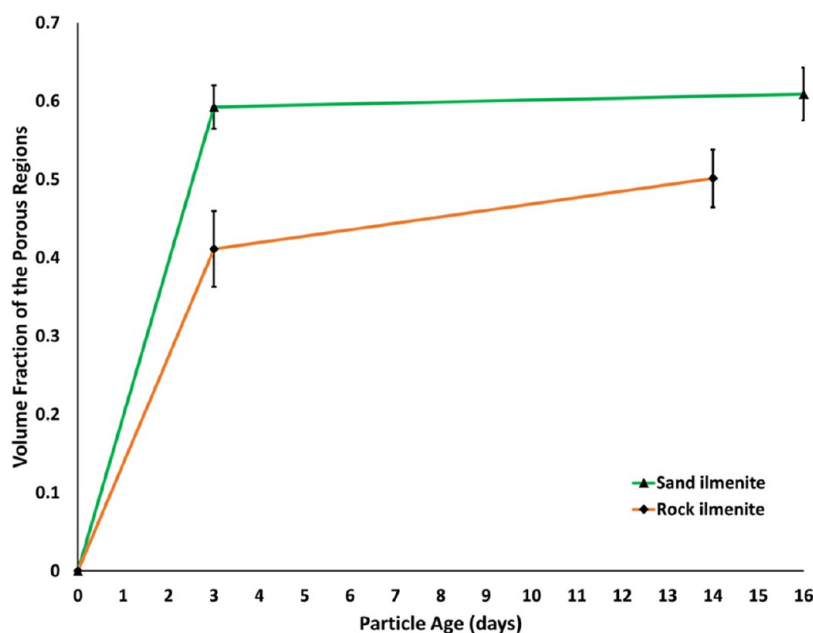


**Figure 14.** Average volume fraction of the porous regions for sand ilmenite bed particles taken at the fresh state, after 3 days and after 16 days, and rock ilmenite bed particles taken at the fresh state, after 3 days and after 14 days from the FBC process measured through XMT analysis. The error bars show 90% confidence interval for the measured data.

aggravation occurred in the early stages of the combustion process.

Formation of the porous regions in the bed particles compromises their structural integrity, leading to a decrease in the mechanical resistance. Therefore, bed particles with increased porosity become more susceptible to breakdown or fragmentation in these regions under external forces in the fluidized bed environment.

Previous studies have demonstrated that the formation of an outer bed particle layer around ilmenite particles acts as a barrier, inhibiting the outward migration of iron. As a result of

the limited outward diffusion, iron seeks alternative pathways for migration, often utilizing the cracks that connect to the surface.<sup>23</sup> It is plausible that the lower volume fraction of the porous regions observed in rock ilmenite could be attributed to the more protective effect exerted by the thicker surface layer. Therefore, the thicker layer formed on rock ilmenite bed particles may reasonably contribute to the observed lower volume fraction of the porous regions.

**3.2.2.2. Iron-Rich Islands.** Observation of SEM-EDS analysis together with XMT images revealed that Fe could also locally accumulate in the bed particle core. SEM-EDS

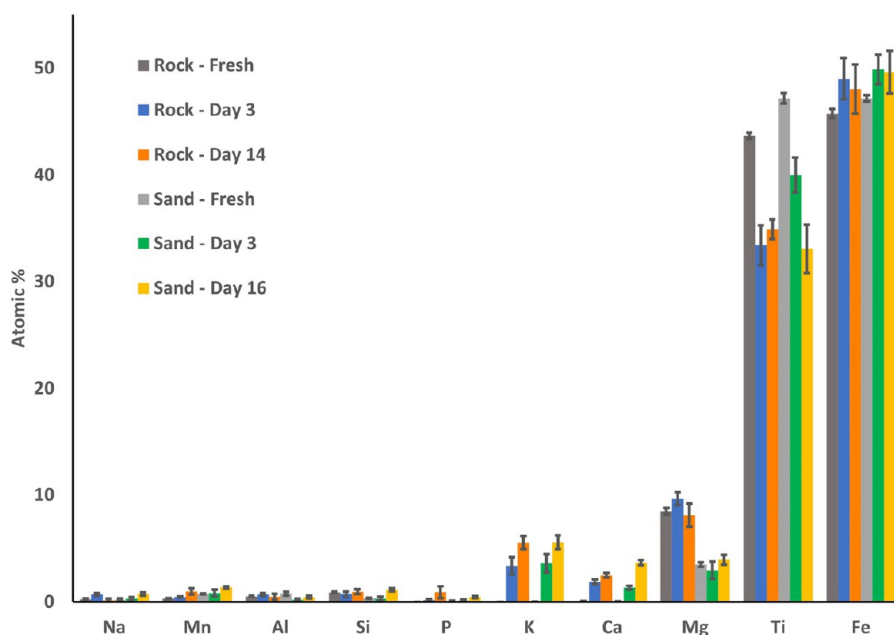


**Figure 15.** Average elemental composition of the fresh bed materials, the iron-rich islands in sand ilmenite bed samples taken after 3 and 16 days, and the iron-rich islands in rock ilmenite bed samples taken after 3 and 14 days from the FBC process. The values are on a C- and O-free basis, presented in at%, and obtained through SEM-EDS. The error bars show 90% confidence interval for the measured data.

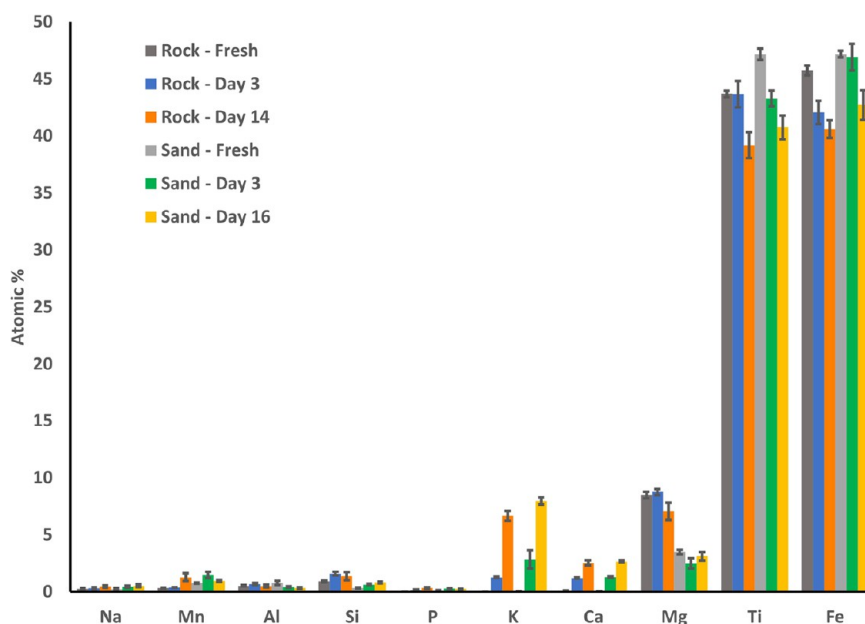


**Figure 16.** Average elemental composition of the fresh bed materials, the rigid bed core in sand ilmenite bed samples taken after 3 and 16 days, and the rigid bed core in rock ilmenite bed samples taken after 3 and 14 days from the FBC process. The values are on a C- and O-free basis, presented in at. % and obtained through SEM-EDS. The error bars show 90% confidence interval for the measured data.

analysis revealed that the brightest regions within the bed particles (Figure 12) possess locally elevated concentrations of iron (Figure 15).

The average volume fraction of iron-rich islands remained nearly constant for both sand and rock ilmenite bed particles after 3 days. However, for the oldest rock ilmenite bed particles (after 16 days), the average volume fraction of the iron-rich islands was 1.4%, nearly double that of sand ilmenite after 14 days, which recorded an average volume fraction of 0.69%. The lower occurrence of iron-rich islands within sand ilmenite bed particles implies that sand ilmenite may exhibit a higher

susceptibility to the outward migration of iron compared with rock ilmenite.

**3.2.2.3. Rigid Bed Core.** The rigid bed core refers to areas inside the bed particles that retained an appearance almost identical with that of the fresh bed material. However, as observed in Figure 16, traces of the ash-forming elements were also detected in these regions. In fact, this phase contrasts with the porous regions, where visible structural changes were evident.

Figure 17 illustrates the temporal changes in the average volume fractions of the rigid bed core areas for both bed types.

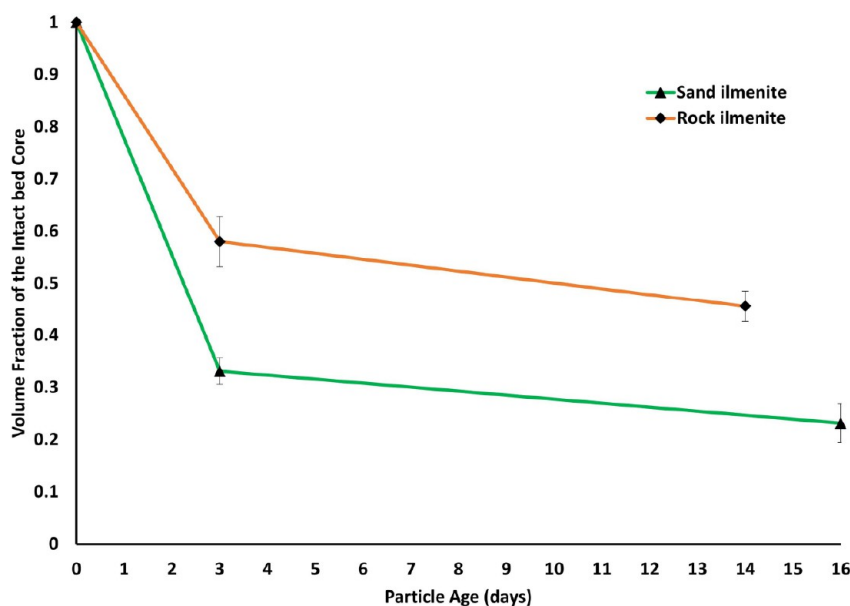


**Figure 17.** Average volume fraction of the rigid bed core for sand ilmenite bed particles taken at the fresh state, after 3 days and after 16 days, and rock ilmenite bed particles taken at the fresh state, after 3 days and after 14 days, from the FBC process measured through XMT analysis. The error bars show 90% confidence interval for the measured data.

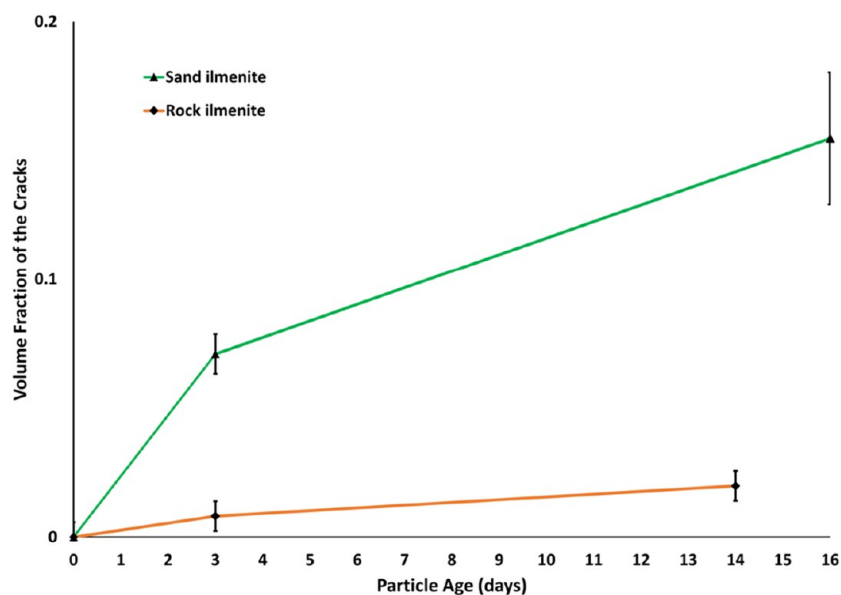


**Figure 18.** Average volume fraction of the cracks for sand ilmenite bed particles taken at the fresh state, after 3 days and after 16 days, and rock ilmenite bed particles taken at the fresh state, after 3 days and after 14 days from the FBC process measured through XMT analysis. The error bars show 90% confidence interval for the measured data.

ANOVA analysis demonstrated a significant difference in the average values for both bed types over time. Subsequent Post analysis with a *t*-test further revealed that the difference in the values persisted even after 3 days. However, the majority of the changes happened in the first 3 days of the combustion process, as can be observed in Figure 17.

**3.2.2.4. Crack Formation.** Formation of the cracks was noticeable after 3 days in both sand and rock ilmenite bed particles (Figures 5b and 6b). As the particles aged, these cracks became more widespread and increasingly propagated throughout the bed particle. Notably, the sand ilmenite particles exhibited a higher frequency of cracks compared with the rock ilmenite particles (Figures 5c and 6c). Cracks in the longest exposed particles began to bridge with each other,

which probably contributed to the fragmentation of the bed material into finer particles. This observation aligns with the findings reported in the previous study.<sup>21</sup>

Figure 18 displays crack development for both the sand and rock ilmenite bed types over time. The data highlighted a significantly higher volume fraction of the cracks in sand ilmenite compared to rock ilmenite bed particles. These observations align with previous findings that cracks propagate more extensively in sand ilmenite, leading to the disintegration of aged sand particles into multiple smaller fragments.<sup>21</sup> In contrast, rock ilmenite tends to have fewer cracks, resulting in the breakage of the particle into comparatively fewer but larger fragments.<sup>21</sup> ANOVA analysis followed by a *t*-test on the results for sand ilmenite revealed that there was a significant

difference in the average values over time. Conversely, for rock ilmenite, no significant difference was noted after a 3-day period.

Observation of SEM and 2D cross-sectional XMT images of both bed types revealed that most of the cracks aligned closely with the porous regions, implying that porous regions may act as transitional phases between the rigid bed core areas and the cracks. The relatively stable volume fraction of the porous regions observed after 3 days (Figure 14) does not necessarily indicate that the porous regions were not propagating any longer. Instead, it might suggest reaching an equilibrium state between regions evolving as porous and those progressing into cracks. To further support this hypothesis, it is valuable to observe the changes in the average volume fraction of the rigid bed core areas of the particle core, depicted in Figure 17, and compare them with the trend witnessed for the cracks in Figure 18. The figures illustrate a decrease in the average volume fraction of the rigid bed core areas (Figure 17), which correlates with the simultaneous increase in the average volume fraction of the cracks and voids (Figure 18). This underscores that the process of mechanical degradation was ongoing, even though the volume fraction of the porous regions remained nearly constant. The capability of XMT to generate three-dimensional images of bed particles, coupled with the ability to examine all 2D cross-sections from various directions, allowed for unique investigation and assisted in conducting a thorough study into how crack formation is related to the geometry of bed particles. In both types of bed particles, it was found that a significant number of cracks originated from or were connected to the concave areas on the bed particle surface (Figures 19 and 20). This is in line with

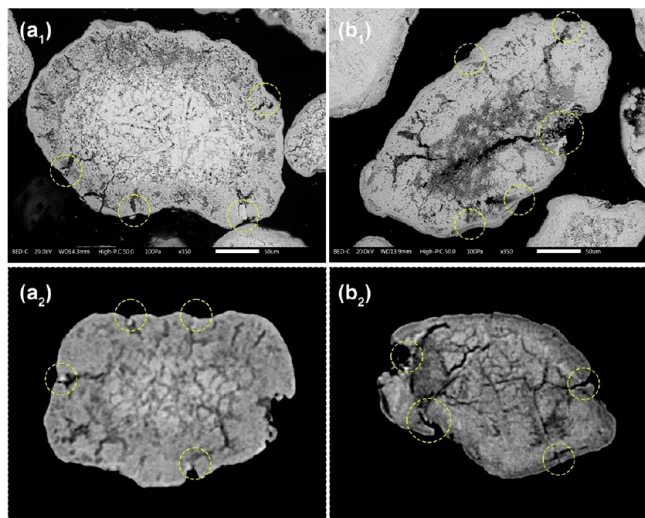


**Figure 19.** SEM (1) and 2D XMT (2) image of cross-sections from typical sand ilmenite bed particles taken after 3 days (a) and 16 days (b) from the FBC process. The yellow dashed circles show cracks connected to the concave areas.

previous findings on crack development in bed particles utilized in FB systems, which indicates a consistent pattern in the behavior of crack development in relation to the bed particles' surface geometry.<sup>27</sup>

Based on the performed analysis, it can be summarized that there is a cumulative impact of transformations that the particles undergo during their exposure to FBC conditions. These transformations can be broadly classified into two

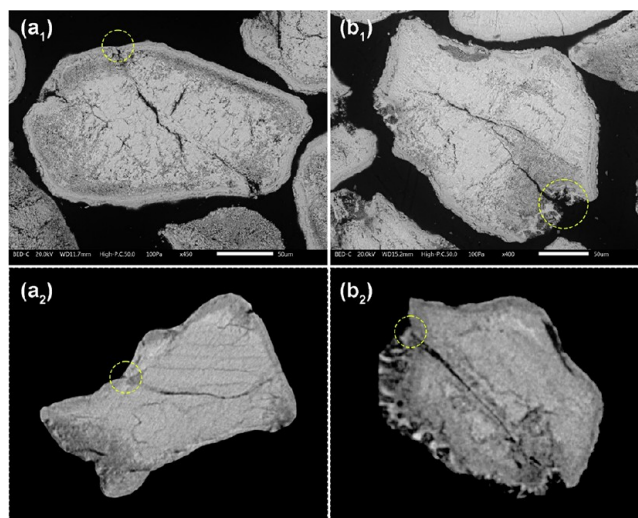


**Figure 20.** SEM (1) and 2D XMT (2) image of cross-sections from typical rock ilmenite bed particle taken after 3 (a) and 14 days (b) from the fluidized bed combustion process. The yellow dashed circles show cracks connected to the concave areas.

categories: surface alteration (also known as the surface layer formation) and internal morphological deviations (i.e., the porosity aggravation and the crack development). The surface alteration predominantly affects interactions between the bed material and the fuel-derived ash compounds, while the internal morphological deviations substantially affect the internal integrity of the bed particles. It is important to note that even though the transformations are classified in two different types, there is an interconnection between the types, and the internal morphological deviations could potentially be a consequence of the initial surface alteration, indicating a complex, interdependent progression of the bed particle transformations.

The morphological transformations within ilmenite bed particles, induced by layer formation, are illustrated in Figures 21 and 22. These figures show 3D representations of the surface layer on typical sand and rock ilmenite particles complemented by 3D XMT images that reveal the heterogeneous internal structures. These structures include distinct regions such as the porous areas, the rigid bed cores, the iron-rich islands, and the cracks. Additionally, to convey the spatial distribution of these diverse regions within the bed particle, 2D XMT images of different cross sections are also provided.

For both sand and rock ilmenite, it could be observed that the porous region predominantly occupied the outermost layer, situated just beneath the formed surface layer. This observation aligns with previous research on the formation of surface layers in ilmenite particles.<sup>23</sup> Notably, in regions where the surface layer was absent, there was a pronounced development of the porosity extending into the core of the bed particle. This absence of layer was primarily noted in the concave regions of the particle surface, leading to a greater distribution of the porous regions in the concavities, while the rigid bed core was more prevalent in the convex surface regions. Furthermore, the discussion of crack formation highlighted a similar pattern. Cracks, analogous to the porous regions, were more prevalent near concave surfaces. In contrast, the iron-rich islands were predominantly located in areas covered by the surface layer, which acted as a barrier and

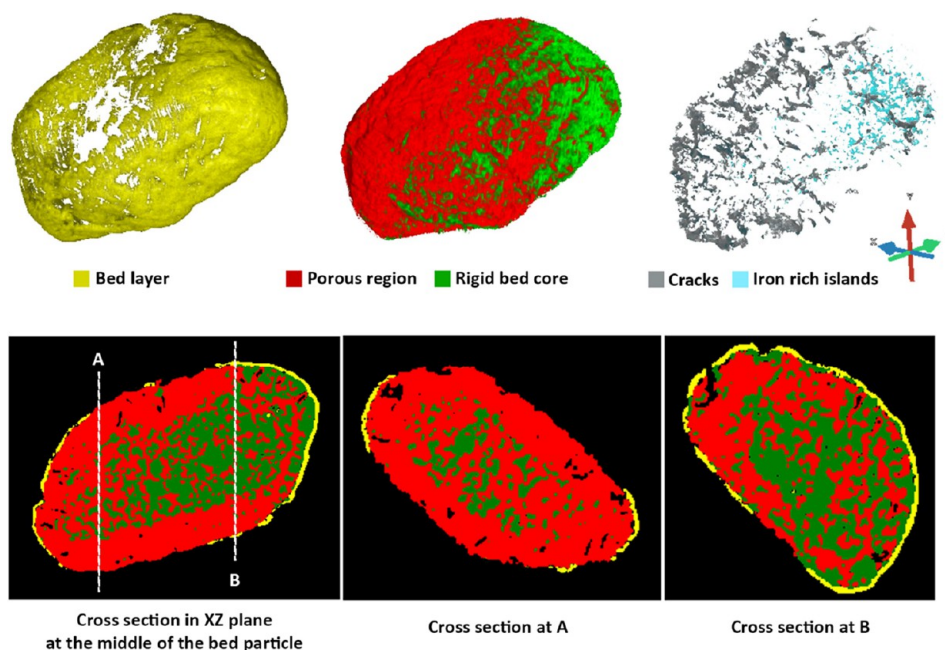


**Figure 21.** XMT analysis revealing the distribution of different internal structures of a typical sand ilmenite bed particle taken after 3 days from the FBC process (lower figures) in comparison to the bed particle layer distribution on the bed particle surface (upper figures).

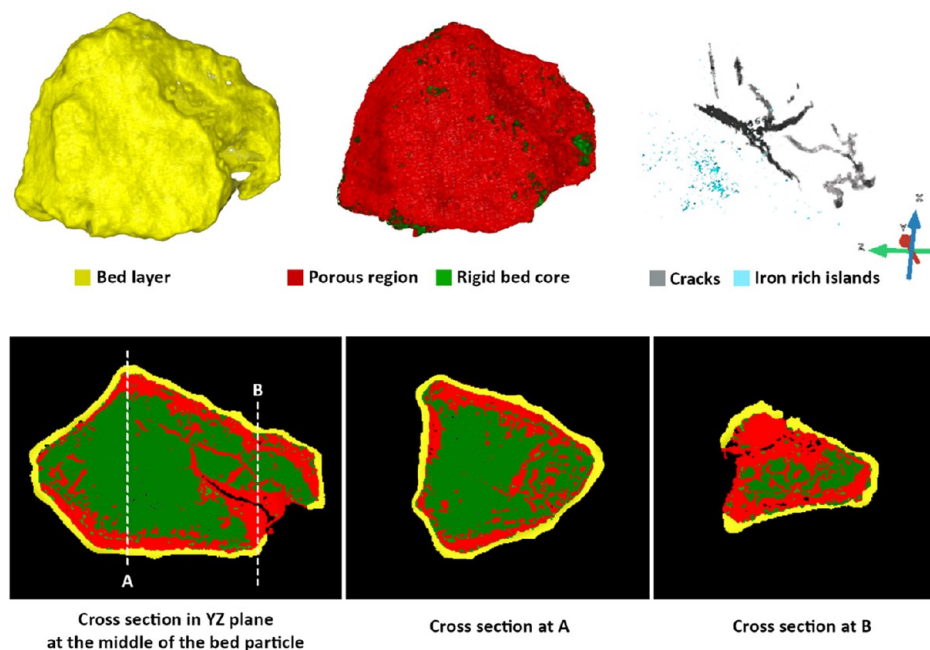


**Figure 22.** XMT analysis revealing the distribution of different internal structures of a typical rock ilmenite bed particle taken after 3 days from the FBC process (lower figures) in comparison with the distribution of the bed particle layer on the bed particle surface (upper figures).

prevented the migration of Fe from the bed core. This intricate interplay of structural features within the bed particles underscores the complex dynamics of layer formation and its impact on the internal morphology of ilmenite bed particles.

As these structural changes accumulate and intensify over time, they can profoundly influence the mechanical strength and stability of the bed material. This gradual and continuous degradation is crucial as it directly affects the performance and durability of the bed material in practical applications.

**3.3. General Discussion and Practical Implications.** A thorough analysis of the results from this study and previous

research on ilmenite bed particles<sup>23,24</sup> indicates that the Fe migration contributes significantly to the ongoing degradation of both sand and rock ilmenite bed particles. However, the degradation process could be dissected into two separate stages. Initially, the process is primarily influenced by the development of the bed particle layer and the outward migration of Fe. As the layer forms (predominantly on convex areas), it acts as a barrier, hindering further migration of Fe toward the particle surface. Consequently, for aged particles, the outward migration of Fe continues via new routes through the concave areas on the bed particle surface, where the

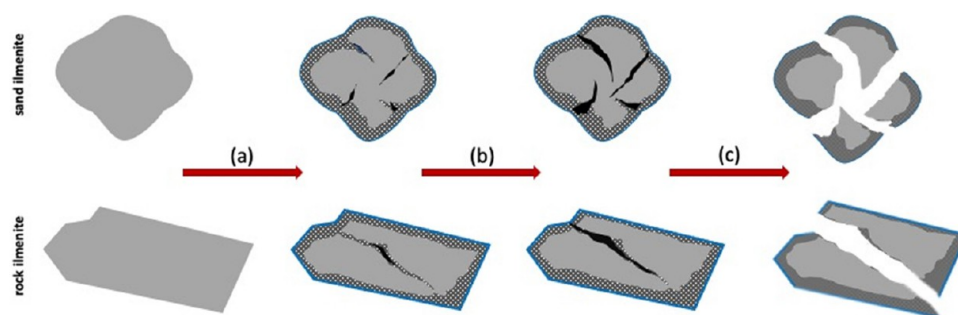


**Figure 23.** Schematic representation of the particle degradation mechanism in sand and rock ilmenite bed particles during the FBC of woody biomass. (a) Formation of the bed particle layer, appearance of the porous regions and some cracks, (b) further propagation of the porous regions and development of the cracks toward concave sites on the surface, and (c) breakage of the bed particles into finer fragments.

formed layer is thinner. The Fe migration further propagates the porous regions in the particle core. Alongside, the expansion of cracks, especially through these porous regions, becomes more pronounced, with some fractures extending to surface concaves and ultimately leading to particle fragmentation.

Figure 23 schematically demonstrates the above-mentioned degradation process. Sand ilmenite is characterized by more distinguished convex and concave features on the surface. The layer predominantly covers the convex regions, leaving the concave areas exposed to further depletion of Fe. This exposure facilitates the propagation of the porous regions within the bed particles, parallel to the formation of multiple cracks extending from the concave surfaces, which finally split the bed particles into multiple fine fragments.

In contrast, rock ilmenite, with comparatively fewer convex and concave features on its surface, exhibits different behavior. The bed particle layer forms uniformly over the flat surfaces, effectively shielding the core of the bed particles from further Fe depletion. Consequently, the presence of this uniform bed particle layer limits the pathways for the crack formation, resulting in fewer cracks compared to sand ilmenite. It should be noted that the formation of a thicker and more uniformly distributed bed particle layer on rock ilmenite bed particles while enhancing their durability through the fluidized bed combustion process, might also impact their oxygen-carrying capacity.<sup>23,24</sup> This, in turn, could potentially affect the overall efficiency of the combustion process by comparatively limiting the access of iron to the bed particle surface. While this aspect falls outside the scope of the current study, it remains an important consideration for subsequent research.

The findings from this study show that there is an interconnection between the elemental mobility and morphological properties, potentially influencing the oxygen carrying ability. The combined impact of these factors may contribute to a reduction in the bed material's lifespan. Understanding the mechanisms governing the chemical and structural evolution of particles can aid in predicting the optimal use of bed materials and subsequently influence their treatment for extended durability.

These observations suggest that even though sand and rock ilmenite show similar compositions, rock ilmenite, with its lower tendency toward fragmentation and its more robust mechanical stability, stands out as the better choice for fluidized bed combustion.

#### 4. CONCLUSIONS

The role of particle geometry on the structural integrity of sand and rock ilmenite bed particles and its effect on layer formation, Fe mobility, and bed particle disintegration were investigated under oxygen carrier-aided wood combustion conditions in a 12 MW<sub>th</sub> CFB boiler. The similar chemical composition of the two bed types allowed a focused comparison based on their differing morphological and mechanistic features. Variations in particle sphericity and surface morphology, along with the development in the chemical composition and volume fraction of the porous, the cracks, and the iron-enriched regions identified within the bed particles, were investigated through SEM-EDS and XMT of bed particle samples taken after different time intervals from the conversion process.

The principal conclusions of this study on the comparative structural integrity of sand and rock ilmenite bed particles are as follows:

1. Over time, the sphericity of sand ilmenite particles diminishes, whereas the shape of rock ilmenite particles remains unchanged.
2. The average specific surface area of sand ilmenite bed particles progressively grows throughout the combustion process, establishing a larger interaction front for elemental mobility both inward and outward from the bed particle surface. In contrast, the average specific surface area of rock ilmenite bed particles remains constant over time.
3. For sand ilmenite, the bed particle layer mainly forms on the convex areas, while in the concave areas, the bed particle layer is very thin or does not exist. This leads to a nonuniform distribution of the bed layer across the bed particle surface. Conversely, with rock ilmenite, where convex and concave features occur infrequently, the bed particle layer exhibits a more uniform distribution on the flat surfaces of the bed particles.
4. Cracks predominantly occur in connection to the concave regions on the bed particle surface.
5. After 3 days, the Ca-rich layer observed on rock ilmenite bed particles is thicker compared to that on sand ilmenite. This thicker layer in rock ilmenite provides enhanced protection against the outward migration of Fe more effectively than in sand ilmenite. Moreover, there is a considerably lower frequency of concave areas on rock ilmenite bed particles compared to sand ilmenite. Consequently, rock ilmenite bed particles exhibit a lower average volume fraction of both porous regions and

cracks, resulting in a structure less prone to particle breakage than sand ilmenite.

## AUTHOR INFORMATION

### Corresponding Author

Ali Valizadeh – Energy Engineering, Division of Energy Science, Luleå University of Technology, SE-97187 Luleå, Sweden; [orcid.org/0000-0003-1203-0410](https://orcid.org/0000-0003-1203-0410); Phone: +46 920 49 2440; Email: [ali.valizadeh@ltu.se](mailto:ali.valizadeh@ltu.se)

### Authors

Robin Faust – Department of Chemistry and Chemical Engineering, Chalmers University of Technology, SE-412 96 Gothenburg, Sweden; [orcid.org/0000-0001-5614-3578](https://orcid.org/0000-0001-5614-3578)

Nils Skoglund – Department of Applied Physics and Electronics, Umeå University, SE-90187 Umeå, Sweden; [orcid.org/0000-0002-5777-9241](https://orcid.org/0000-0002-5777-9241)

Fredrik Forsberg – Division of Fluid and Experimental Mechanics, Luleå University of Technology, SE-97187 Luleå, Sweden

Marcus Öhman – Energy Engineering, Division of Energy Science, Luleå University of Technology, SE-97187 Luleå, Sweden

Pavleta Knutsson – Department of Chemistry and Chemical Engineering, Chalmers University of Technology, SE-412 96 Gothenburg, Sweden

Complete contact information is available at:

<https://pubs.acs.org/10.1021/acs.energyfuels.4c00658>

### Notes

The authors declare no competing financial interest. During the preparation of this work the first author used ChatGPT in order to enhance the fluency, language structuring and overall readability of the text. After using this tool, the first author reviewed and edited the content as needed and takes full responsibility for the content of the publication.

## ACKNOWLEDGMENTS

The financial supports provided by the Swedish Energy Agency project no. P46533-1 and the Swedish Research Council, project no. 2023-03500 are gratefully acknowledged. The authors would also like to acknowledge the LUMIA research infrastructure at Luleå University of Technology for the access to the SEM/EDS and X-ray microtomography systems, along with help and guidance during the measurements.

## REFERENCES

- (1) Yao, S.; Zhang, S.; Zhang, X. Renewable energy, carbon emission and economic growth: A revised environmental Kuznets Curve perspective. *Journal of Cleaner Production* **2019**, *235*, 1338–1352.
- (2) Sayed, E. T.; Olabi, A. G.; Alami, A. H.; Radwan, A.; Mdallal, A.; Rezk, A.; Abdelkareem, M. A. Renewable energy and energy storage systems. *Energies* **2023**, *16* (3), 1415.
- (3) Deshmukh, M. K. G.; Sameeroddin, M.; Abdul, D.; Sattar, M. A. Renewable energy in the 21st century: A review. *Mater. Today: Proc.* **2023**, *80*, 1756–1759.
- (4) Liu, Z.; Deng, Z.; Davis, S.; Ciais, P. Monitoring global carbon emissions in 2022. *Nature Reviews Earth & Environment* **2023**, *4* (4), 205–206.
- (5) Blum, M.; Lövbrand, E. The return of carbon offsetting? The discursive legitimization of new market arrangements in the Paris climate regime. *Earth Syst. Governance* **2019**, *2*, No. 100028.

(6) Gao, S.; Li, M.-Y.; Duan, M.-S.; Wang, C. International carbon markets under the Paris Agreement: Basic form and development prospects. *Advances in Climate Change Research* **2019**, *10* (1), 21–29.

(7) Khatiwada, D.; Kapothanilath, A.; Harahap, F. M.; Sousa, C. I. N. D. L.; De Almeida, P. H. Towards a bio-economy—An integrated approach for biogas utilisation and policy analysis in the Nordic Region. *Fast Track to*, 116.

(8) Kożuch, A.; Cywicka, D.; Adamowicz, K.; Wieruszewski, M.; Wysocka-Fijorek, E.; Kielbasa, P. The Use of Forest Biomass for Energy Purposes in Selected European Countries. *Energies* **2023**, *16* (15), 5776.

(9) Böhlenius, H.; Öhman, M.; Granberg, F.; Persson, P.-O. Biomass production and fuel characteristics from long rotation poplar plantations. *Biomass and Bioenergy* **2023**, *178*, No. 106940.

(10) Manaf, N. A.; Milani, D.; Abbas, A. Assessing the Current State of Biomass Gasification Technology in Advancing Circular Economies: A Holistic Analysis from Techno-Economic-Policy Perspective in Malaysia and Beyond. *Chem. Eng. Res. Des.* **2023**, *199*, 593–619, DOI: [10.1016/j.cherd.2023.10.023](https://doi.org/10.1016/j.cherd.2023.10.023).

(11) Anthony, E. fluidized bed combustion of alternative solid fuels; status, successes and problems of the technology. *Prog. Energy Combust. Sci.* **1995**, *21* (3), 239–268.

(12) Motta, I. L.; Miranda, N. T.; Maciel Filho, R.; Wolf Maciel, M. R. Biomass Gasification in fluidized beds: A review of biomass moisture content and operating pressure effects. *Renewable and Sustainable Energy Reviews* **2018**, *94*, 998–1023.

(13) Geyter, S. D.; Öhman, M.; Boström, D.; Eriksson, M.; Nordin, A. Effects of Non-Quartz Minerals in Natural Bed Sand on Agglomeration Characteristics during fluidized Bed Combustion of Biomass Fuels. *Energy Fuels* **2007**, *21*, 2663–2668.

(14) He, H.; Ji, X.; Boström, D.; Backman, R.; Öhman, M. Mechanism of quartz bed particle layer formation in fluidized bed combustion of wood-derived fuels. *Energy Fuels* **2016**, *30* (3), 2227–2232.

(15) He, H.; Boström, D.; Öhman, M. Time Dependence of Bed Particle Layer Formation in fluidized Quartz Bed Combustion of Wood-Derived Fuels. *Energy Fuels* **2014**, *28* (6), 3841–3848.

(16) He, H.; Skoglund, N.; Öhman, M. Time-Dependent Crack Layer Formation in Quartz Bed Particles during fluidized Bed Combustion of Woody Biomass. *Energy Fuels* **2017**, *31* (2), 1672–1677.

(17) Li, L.; Mao, J.; Tang, W.; Sun, G.; Gu, Q.; Lu, X.; Shao, K.; Chen, Y.; Duan, L. Experimental study on coal combustion by using the ilmenite ore as active bed material in a 0.3 MWth circulating fluidized bed. *Fuel* **2023**, *342*, No. 127007.

(18) Thunman, H.; Lind, F.; Breitholtz, C.; Berguerand, N.; Seemann, M. Using an oxygen-carrier as bed material for combustion of biomass in a 12-MWth circulating fluidized-bed boiler. *Fuel* **2013**, *113*, 300–309.

(19) Daneshmand-Jahromi, S.; Sedghkerdar, M. H.; Mahinpey, N. A review of chemical looping combustion technology: Fundamentals, and development of natural, industrial waste, and synthetic oxygen carriers. *Fuel* **2023**, *341*, No. 127626.

(20) Duan, L.; Li, L. The Evolution of OCAC and Its Working Principles. In *Oxygen-Carrier-Aided Combustion Technology for Solid-Fuel Conversion in fluidized Bed*; Springer, 2023; pp 9–17.

(21) Corcoran, A.; Knutsson, P.; Lind, F.; Thunman, H. Comparing the structural development of sand and rock ilmenite during long-term exposure in a biomass fired 12 MWth CFB-boiler. *Fuel Process. Technol.* **2018**, *171*, 39–44.

(22) Bartocci, P.; Abad, A.; Flores, A. C.; De Las Obras Loscertales, M. ilmenite: A promising oxygen carrier for the scale-up of chemical looping. *Fuel* **2023**, *337*, No. 126644.

(23) Priščák, J.; Valizadeh, A.; Öhman, M.; Hofbauer, H.; Kuba, M. Effect of time-dependent layer formation on the oxygen transport capacity of ilmenite during combustion of ash-rich woody biomass. *Fuel* **2023**, *353*, No. 129068.

(24) Corcoran, A.; Knutsson, P.; Lind, F.; Thunman, H. Mechanism for migration and layer growth of biomass ash on ilmenite used for

oxygen carrier aided combustion. *Energy Fuels* **2018**, *32* (8), 8845–8856.

(25) Valizadeh, A.; Skoglund, N.; Forsberg, F.; Lycksam, H.; Öhman, M. A comparative study in 3D of bed particle layer characteristics in quartz and K-feldspar from fluidized bed combustion of woody biomass using X-ray microtomography. *Fuel* **2023**, *342*, No. 127707.

(26) Faust, R.; Valizadeh, A.; Qiu, R.; Tormachen, A.; Maric, J.; Vilches, T. B.; Skoglund, N.; Seemann, M.; Halvarsson, M.; Öhman, M. Role of surface morphology on bed material activation during indirect Gasification of wood. *Fuel* **2023**, *333*, No. 126387.

(27) Valizadeh, A.; Skoglund, N.; Forsberg, F.; Lycksam, H.; Öhman, M. Role of surface morphology in bed particle layer formation on quartz bed particles in fluidized bed combustion of woody biomass. *Fuel* **2024**, *357*, No. 129702.

(28) Scala, F. *Fluidized bed technologies for near-zero emission combustion and Gasification*; Elsevier, 2013.

(29) Lain, S.; Castang, C.; García, D.; Sommerfeld, M. Sphericity based correlations for flow resistance coefficients of non-spherical particles of irregular shape beyond the Stokes regime. *Chem. Eng. Sci.* **2023**, *282*, No. 119288.

(30) Yogi, J.; Dubey, P.; Khatoun, S.; Iyer, K.; Kumar, S.; Anand, A. Effect of non-sphericity of a narrow-sized binary mixture on mixing in convective vibrated packed bed using Discrete Element Method. *Powder Technol.* **2023**, *426*, No. 118600.

(31) Cruz-Matías, I.; Ayala, D.; Hiller, D.; Gutsch, S.; Zacharias, M.; Estradé, S.; Peiró, F. Sphericity and roundness computation for particles using the extreme vertices model. *Journal of computational science* **2019**, *30*, 28–40.

(32) Onsager, L. The effects of shape on the interaction of colloidal particles. *Ann. N.Y. Acad. Sci.* **1949**, *51* (4), 627–659.

(33) Gahn, C.; Krey, J.; Mersmann, A. The effect of impact energy and the shape of crystals on their attrition rate. *Journal of crystal growth* **1996**, *166* (1–4), 1058–1063.

(34) Ray, Y.-C.; Jiang, T.-S.; Wen, C. Particle attrition phenomena in a fluidized bed. *Powder Technol.* **1987**, *49* (3), 193–206.

(35) Rutherford, A. *ANOVA and ANCOVA: a GLM approach*; John Wiley & Sons, 2011.

(36) King, A. P.; Eckersley, R. *Statistics for biomedical engineers and scientists: How to visualize and analyze data*; Academic Press, 2019.

(37) Mgangira, M. B.; Anochie-Boateng, J.; Komba, J. J. *Quantification of aggregate grain shape characteristics using 3-D laser scanning technology*, 2013.